CRYSTAL GROWTH & DESIGN

pubs.acs.org/crystal

Article

Multifunctional Fluorescent Tetraphenylethene-Based Reversible Mechanochromism for Highly Selective Detection of MnO_4^- in Aqueous Media and Green Organic Light Emitting Diode Applications

Published as part of a Crystal Growth and Design virtual special issue Celebrating John N. Sherwood, Pioneer in Organic and Molecular Crystals

Kishor S. Jagadhane, Ray J. Butcher, Tukaram D. Dongale, Kiran A. Nirmal, Govind B. Kolekar, Mohaseen S. Tamboli, Tae Geun Kim, Sunita Salunke-Gawali, and Prashant V. Anbhule*

Cite This: *Cryst. Growth Des.* 2023, 23, 4164–4179

Read Online

ACCESS | Metrics & More | Article Recommendations | Supporting Information

ABSTRACT: Ethyl 2-cyano-3-(4-(1,2,2-triphenylvinyl) phenyl) acrylate (TPE-SKJ), a newly synthesized luminogen based on tetraphenylethene, with single crystal analysis exhibits photophysical phenomena such as aggregation-induced emission (AIE); reversible mechanochromic, solvatochromic, organic light emitting diode; and chemical sensing in aqueous media with great selectivity and a low limit of detection. The synthesized material demonstrates high selectivity and sensitivity capacity for sensing MnO_4^- in mixed aqueous media (water/acetonitrile, v/v, 9/1). The detection limit for MnO_4^- was found to be 0.086009 μg mL^{-1} with a quantum yield (Φ) of 11%. Moreover, we employed TPE-SKJ material in an organic light-emitting diode (OLED) as an emissive layer. The device shows a maximum of 1.62% external quantum efficiency, higher than nondoped emitting layer-based green OLEDs. The present results will encourage ongoing research into the design of novel stimuli-responsive organic materials with switchable properties based on their supramolecular interactions for numerous applications.

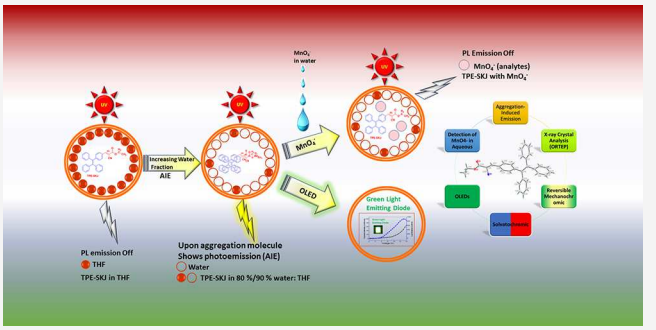

1. INTRODUCTION

Aggregation-induced emission (AIE), a type of photophysical phenomenon connected to the aggregation of the chromophore moiety, was first proposed by Prof. B. Z. Tang and his team in 2001. In an aggregation-induced emission (AIE) mechanism, the water content in the mixture affects how quickly weak or nonemissive luminogens aggregate to become emissive; it means aggregation-induced emission means weak or nonemissive luminogens become emissive upon aggregation. Early research on AIE indicated that scientists were more interested in how a substance's molecular structure might affect it. As time went on, it was discovered that not all emission phenomena, particularly polymorphisms with various emissive features, could be described by molecular structure. In contrast, AIE exhibited a normal solid-state luminescence behavior, and the change in molecular packing from intense $\pi-\pi$ stacking to a suppressed one was the primary cause of the transition from ACQ to AIE. As a result, researchers started to concentrate more on molecule packing than molecular structure.[1−3] The tetraphenylethene-based luminogens show amazing photophysical phenomena such as aggregation-induced emission, solvatochromism, reversible mechanochromic, etc., which have very useful applications in diverse fields.[4]

Because of their use in optical information storage camouflage, mechanical sensors, memory chips, and security papers, luminogens with reversible stimulus-responsive switching in the solid state have drawn a great deal of attention.[5−8] Industry and academia have recently become enthusiastic about the successful applications of various aggregation-induced emission (AIE)-based reversible mechanochromic (MC) materials in cutting-edge nanotechnologies.[9−11] Contrary to conventional fluorophores, AIEgens have had the unique property of an emission strongly in the aggregated state (solid) despite being nonemissive in the solution state, due to restrictions on intramolecular rotations (RIR) or restrictions

Received: January 1, 2023
Revised: May 11, 2023
Published: May 30, 2023

https://doi.org/10.1021/acs.cgd.3c00002
Cryst. Growth Des. 2023, 23, 4164−4179

Scheme 1. Synthetic Route of TPE-SKJ [(*E*)-Ethyl 2-cyano-3-(4-(1,2,2-triphenylvinyl) phenyl) acrylate (*E*)-ethyl 2-cyanobut-2-enoate]

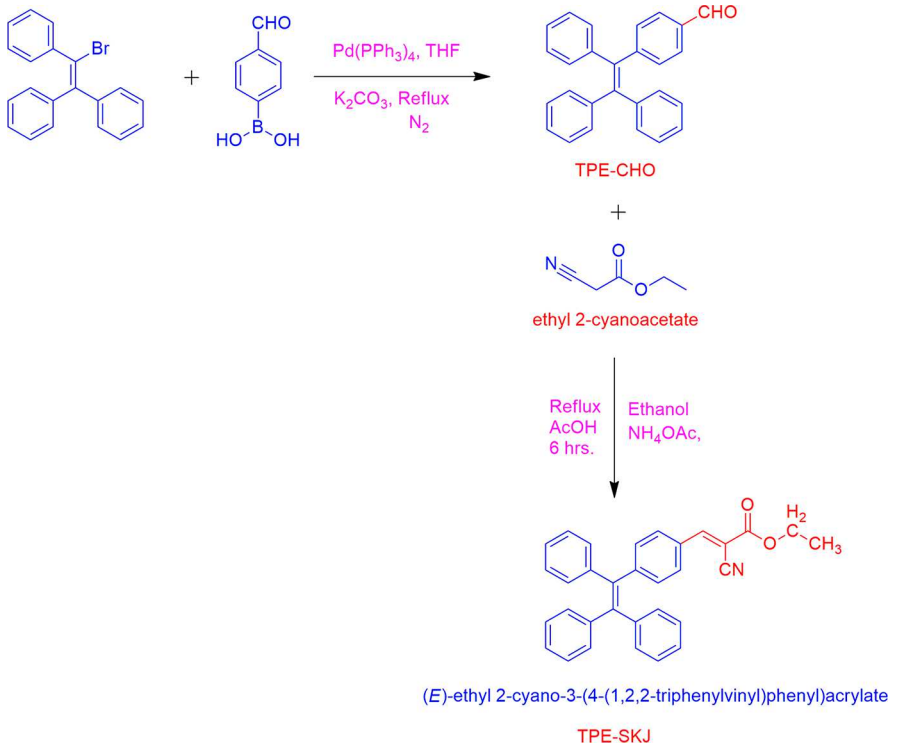

on intramolecular vibrations (RIV) during aggregate formation.[12−14] This fluorogenic material can be adapted to make sensitive "off-on" probes that are biocompatible and selective and exhibit weak fluorescence in aqueous media while activating fluorescence in response to target analytes.[15] Due to their greater photobleaching resistance, AIE probes exhibit higher stability and superior signal reliability when compared to conventional fluorescent probes.[16−19] In addition, the fields of sensing and OLEDs show highly valuable applications for aggregation-induced emission, solvatochromic, and reversible mechanochromic luminogens. Because inorganic hazardous anions are present in significant quantities as a result of global industrialization, we have used the synthesized luminogen for the sensing of anions in an aqueous field with the inspiration of sensing applications.

Inorganic hazardous anions are being discharged into our living environment rapidly due to global industrialization and creating multiple significant environmental and public health consequences. Such species in the ecosystem must be detected and identified even though they are fundamental to our ordinary life and health in trace quantities.[20] As a result, MnO_4^- has drawn considerable attention due to its severe effects on human health and the environment. The US Environmental Protection Agency has identified that it is a significant pollution issue.[21] MnO_4^- exposure in humans can harm the respiratory system and have other unfavorable effects. As a result, scientists are working hard to find clear, simple, and valuable techniques for detecting MnO_4^- at low concentrations.[22] First, we developed a quick and effective sensor for detecting MnO_4 specifically in an aqueous medium. There are very few known organic luminogen sensors for MnO_4 which are used in aqueous media. In comparison, sensors for MnO_4^- and other analytes with lower LODs have been reported by Sun et al.,[20] Su et al.,[23] Huang et al.,[24] Zhang et al.,[25] and Wang et al.,[26] but none of these sensors was successful in detecting MnO_4 ions specifically. A new approach for the sensitive and precise detection of MnO_4 was developed in aqueous media. Many research teams have recently concentrated on detecting heavy metal ions, which are responsible for significant environmental pollution problems and have an effect on human health. Atomic absorption spectrometry (AAS), atomic fluorescence spectroscopy (AFS), inductively coupled plasma mass spectrometry (ICPMS), and X-ray fluorescence spectrometry are some of the analytical techniques that are frequently utilized to detect environmental pollutants. However, these analytical methods could be more practical due to the difficulty of sample preparation, complex instrumentation, and extremely high cost for third-world countries.[25]

Organic light-emitting diodes (OLEDs), having potential applications in flat-panel displays and solid-state lighting, have attracted a lot of attention after Tang et al.'s benchmarking results in 1987.[27] Thermal evaporation, however, makes fabrication more difficult and results in very low utilization of costly light-emitting materials. Processes that utilize solutions, such as spin-coating and inkjet printing, are the most effective at increasing process effectiveness and lowering production costs. Interestingly, small molecules have several inherent benefits over polymers, including simple synthesis, high purity, and clearly defined chemical structures. Consequently, using solution-processable small molecules to make OLEDs is a potential option to improve the chances of producing large-area and inexpensive flat-panel displays and solid-state lighting. AIE-featured luminogens have so far been reported to be efficient electroluminescent materials in large numbers; however, solution-processable AIE materials are still rare and are rarely developed for OLEDs.[27−29]

https://doi.org/10.1021/acs.cgd.3c00002
Cryst. Growth Des. 2023, 23, 4164−4179

In the present work, the synthesized luminogen (TPE-SKJ) was used to detect toxic anions (MnO_4^-), particularly from aqueous media, with naked-eye detection. The synthesized novel organic luminogen is a tetraphenylethene derivative with an ethyl cyano butenoate binder having a quantum yield (Φ) of 11%. This luminogen exhibits remarkable mechanochromic (MC) phenomena and certain photophysical phenomena, such as aggregation-induced emission (AIE), solvatochromism, and reversible mechanochromism. Using various techniques, we studied the synthetic organic luminogen and then used it for selective and sensitive detection of toxic anions (MnO_4^-) in aqueous media. The detection limit for MnO_4^- was found to be 0.086009 μg mL^{-1}. Furthermore, we employed TPE-SKJ material as an emissive layer for an organic light-emitting diode (OLED). The device shows a maximum 1.62% external quantum efficiency, higher than nondoped emitting layer-based green OLEDs.[26,30]

2. EXPERIMENTAL SECTION

2.1. Chemicals and Equipment. All chemicals were used directly from commercial suppliers without further purification. 4-(1,2,2-Triphenyl) benzaldehyde and ethyl cyanoacetate were mixed in the presence of ammonium acetate and acetic acid to synthesize the TPE-SKJ luminogen. Sigma-Aldrich chemicals are used to synthesize a luminogen. The different anion salts, including (SO_4^{-2}, BrO_3^-, S^{-2}, $Cr_2O_7^{-2}$, HPO_4^{-2}, IO_3^-, MnO_4^-, SO_3^{-2}, SCN^-, CO_3^{-2}, CrO_4^-, I^-, etc.) were used in the present study. Additionally, DMSO used was purchased from TCI and Sigma-Aldrich.

The synthesized AIEgen was characterized using different characterization techniques like IR (ATR), ^1H and ^{13}CNMR, and HR-MS spectrometry. An IR spectrum was recorded on a Bruker, Germany (ALPHA) spectrometer with a range of 4000 to 400 cm^{-1}. ^1H NMR spectra were recorded on a 400 MHz Bruker Advance spectrometer and ^{13}C NMR spectra were recorded using 101 MHz spectrometers ($CDCl_3$-*d* or DMSO-d_6 was used as solvent, trimethyl silane as an internal standard). DEPT-135-NMR spectra were recorded on a 400 MHz Bruker Advance spectrometer. A Waters Micromass Q-Tof Micro in ESI-MS mode was used to collect data. Absorption spectra were recorded by the Specord plus UV/vis double-beam spectrophotometer (Analytik Jena), and fluorescence emission was measured on the FP-8300 (Jasco) fluorescence spectrometer. TLC (on the silica-coated aluminum plate) was used to monitor the progression of all the reactions.

2.2. Synthesis of TPE-SKJ ((*E*)-Ethyl 2-cyano-3-(4-(1,2,2-triphenylvinyl) phenyl) acrylate/(*E*)-ethyl 2-cyanobut-2-enoate). *2.2.1. Synthesis of TPE-CHO 4-(1,2,2-Triphenylvinyl) benzaldehyde.* The synthetic route for TPE-CHO is highlighted in Scheme 1. The required starting material TPE-CHO is synthesized by our previous report.[31,32]

1-Bromo-1,2,2-triphenylethylene (335.24 mg, 1.0 mmol) as well as 4-formylphenylboronic acid (179.9 mg, 1.2 mmol) were dissolved in a 20 mL solution of tetrahydrofuran and a 2 M potassium carbonate (K_2CO_3) aqueous solution (7 mL). The entire mixture was stirred for 0.5 h at room temperature under a nitrogen (N_2) atmosphere, then Tetrakis (triphenylphosphine)palladium (0) (0.010 g) was added, and the mixture was allowed to reflux at 80 °C overnight. The progress of the reaction was monitored by TLC; after the completion of the reaction, the solvent was removed under reduced pressure, to form a residue; the formed residue was chromatographed on a silica gel column with *n*-hexane/dichloromethane (V/V 3:1) as eluent to afford a light-yellow powder as a product that is TPE-CHO (346.0 mg, 96% yield).

2.2.2. Synthesis of Desired (E)-Ethyl 2-cyano-3-(4-(1,2,2-triphenylvinyl) phenyl) acrylate (TPE-SKJ)/(E)-ethyl 2-cyanobut-2-enoate. The synthetic route for TPE-SKJ is highlighted in Scheme 1.

Initially, 4-(1,2,2-triphenylvinyl) benzaldehyde (0.1333 g, 0.37 mmol) was dissolved in 5 mL ethanol. In this solution, a mixture of ethyl cyanoacetate (0.33 g, 2.97 mmol) in ammonium acetate (1 g) and 15 mL acetic acid was added. After that, the whole reaction mixture was refluxed at 60 °C for 12 h. After completion of the reaction, the reaction mixture was cooled to room temperature; the yellow precipitate generated was filtered after addition of 30 mL of ice-cold water. The progress of the reaction was monitored by TLC, and the final pale-yellow residue was purified by column chromatography with petroleum ether/ethyl acetate (v/v = 90/10) to afford (*E*)-ethyl 2-cyano-3-(4-(1,2,2-triphenylvinyl) phenyl) acrylate (142.0 mg, 86% yield). The spectroscopic data are provided in the Supporting Information.

2.3. UV−vis and Fluorescence Experiments. The standard solution of anions (100 μg mL^{-1}) was prepared in double-distilled water by adding the desired quantity of salts to the water and allowing them to dissolve. A stock solution of the luminogen (1×10^{-4} M) was prepared in acetonitrile. To develop test solutions for spectral analysis, 1.0 mL (1×10^{-4} M) of luminogen and 1.0 mL (100 μg mL^{-1}) of individual anions were mixed in a test tube. Up to 10 mL of distilled water was added to dilute the test tube, and the solution was allowed to remain for 10 min at room temperature well before the recording of the absorption and fluorescence (emission) spectra.

2.4. Fluorescence Titration for the Detection of MnO_4^- Anion. The 1 mL probe 1 (10^{-4} mol/L) in acetonitrile solution was placed in each test tube of the different set and a fraction of varying concentrations of the aqueous solution of MnO_4^- (1 ppm) ions solution was added. All solutions were diluted to a constant volume. Eventually, all test tube solutions were subjected sequentially for absorption and emission measurement at room temperature. The fluorescence spectra were recorded at $\lambda_{ex.}$ = 417 nm and medium sensitivity with a bandwidth of 10.

2.5. Paper Strips of Luminogen Are Prepared as Follows. Cut pieces of Whatman paper No. 41 were used to make the paper strips. The test strips were made ready by immersing them in a solution of acetonitrile containing synthesized luminogen. The strips were allowed to air-dry. These test strips were designed to find MnO_4^- when other anions were present. The test strips were evaluated using UV light at 365 nm to make straightforward visual detection possible.[33]

2.6. DLS Study. The solution of luminogen was prepared in an acetonitrile:acetonitrile mixture solution, and the anions solution were prepared in the double-distilled water. Lastly, the DLS measurement was carried out initially with only a probe and then the same experimental performance was carried out in the presence of anions (MnO_4^-) solution with a ratio of 1:0.5.[33]

2.7. OLED Device Fabrication. All organic materials were purchased from Ossila. Patterned ITO-coated glass substrates were cleaned sequentially in ultrasonic baths of acetone, methanol, and distilled water. Cleaned glass substrates were dried with nitrogen blow and subjected to UV irradiation for 10 min. A 40 nm layer of poly(3,4-ethylene dioxythiophene)−poly(styrene sulfonic acid) (PEDOT:PSS) was spin-coated at the speed of 3000 rpm for 40 s. Then PEDOT:PSS coated substrates were transferred to a glovebox containing an N_2 atmosphere and heated at 120 ° C for 20 min to remove residual solvents. An organic emissive layer of TPE-SKJ dissolved in acetonitrile was spin-coated at 3500 rpm for 30 s to achieve a thickness of 70 nm. Furthermore, 40-nm-thick TPBi was deposited with a shadow mask by using a vacuum thermal evaporation system (Daedong High Tech, Korea) under a pressure of 8×10^{-7} Torr. Finally, 0.8 nm LiF and 120 nm Al (top cathode) were deposited by using a thermal evaporation system.

2.8. OLED Characterizations. An OLED measurement system (M6100 program, McScience) was used to measure the current density−voltage−luminance (*J*−*V*−*L*), current efficiency (CE), and electroluminescence (EL) spectrum characteristics based on an effective area of 3 cm × 3 cm.

2.9. Experimental Crystal Structure Determination of the Compounds. Data for the TPE-SKJ have been collected on D8 Venture PHOTON 100 CMOS diffractometer using graphite monochromatized Mo−Kα radiation (λ = 0.7107 Å) with exposure/frame = 10 s. The X-ray generator was operated at 50 kV and 30 mA. An initial set of cell constants and an orientation matrix

https://doi.org/10.1021/acs.cgd.3c00002
Cryst. Growth Des. 2023, 23, 4164−4179

Scheme 2. ORTEP of TPE-SKJ[a]

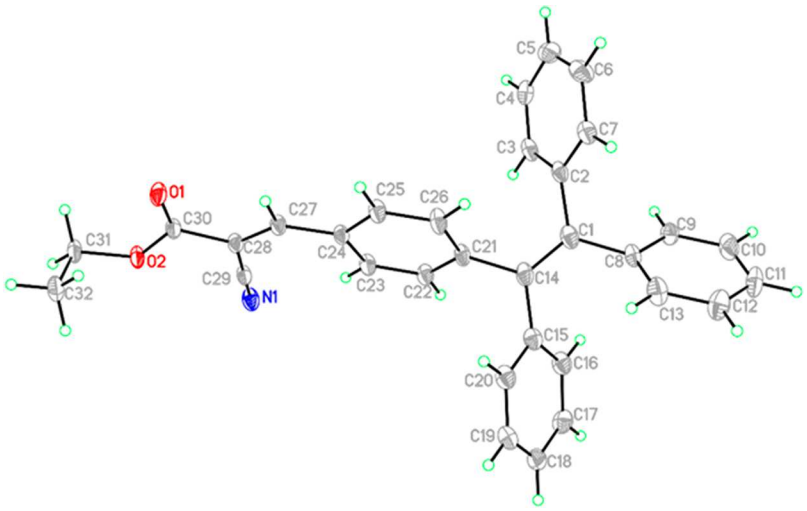

[a]The ellipsoids were drawn with a 50% probability.

were calculated from 24 frames. The optimized data collection strategy consisted of different ϕ and ω scans with 0.5° steps in ϕ/ω. Crystal to detector distance was 5.00 cm with 512 × 512 pixels/frame, Oscillation/frame −0.5°, maximum detector swing angle = −30.0°, beam center = (260.2, 252.5), in-plane spot width = 1.24. Bruker SAINT program carried out data integration, and empirical absorption correction for intensity data was incorporated through Bruker SADABS. The programs are integrated with the APEX II package.[34] The data were corrected for the Lorentz and polarization effects. Further, the structure was solved by the direct method using SHELX-97[35] and finally refined by employing the full-matrix least-squares techniques using anisotropic thermal data for the non-hydrogen atoms on F2. The non-hydrogen atoms were refined anisotropically, whereas the hydrogen atoms were refined at calculated positions as riding atoms with the isotropic displacement parameters[35] and Mercury software programs.[36] The final structures were derived using SHELXTL[37] and PLATON.[38]

3. RESULTS AND DISCUSSION

3.1. Characterization of TPE-SKJ. The details of the synthesis are discussed in the Experimental Section; however, Scheme S2 depicts the full synthetic process for luminogen (TPE-SKJ; Scheme 2). It was completely described by employing physicochemical analysis and spectroscopic methods. This study revealed the successful synthesis of TPE-SKJ. The purity and structure of the luminogen were confirmed by using FT-IR, ^{1}H and ^{13}C NMR, and HR-MS spectrometry (kindly refer to the Supporting Information for more details).

3.2. X-ray Crystallographic Analysis Study. CCDC number 2221617 contains the supplementary crystallographic data for these complexes and can be obtained free of charge from the Cambridge Crystallographic Data Centre via www.ccdc.cam.ac.uk/data_request/cif.

3.2.1. X-ray Crystal Analysis of Desired (E)-Ethyl 2-cyano-3-(4-(1,2,2-triphenylvinyl) phenyl) acrylate (TPE-SKJ)/(E)-ethyl 2-cyanobut-2-enoate. Tpe crystallizes in triclinic space group $P\bar{1}$. The crystal structure data are presented in Table 1. The bond distance of sp^2 carbons C(1) and C(2) is 1.343 Å. The carbonyl bond distances C(30)−O(1) and C(30)−O(2), respectively, are 1.206 and 1.334 Å.The ∠C2−C1−C8 is = 115.28° and ∠C21−C14−C15 is 114.65°. All the phenyl rings are nonplanar to one another.

Table 1. Crystal Data and Structure Refinement for TPE-SKJ

CCDC	2221617	
Empirical formula	$C_{32}H_{25}NO_2$	
Formula weight	455.53	
Temperature	100(2) K	
Wavelength	0.41328 Å	
Crystal system	Triclinic	
Space group	$P\bar{1}$	
Unit cell dimensions	a = 5.5005(3) Å	α = 93.766(2)°
	b = 9.4955(7) Å	β = 94.6790(10)°
	c = 24.5928(16) Å	γ = 105.7450(10)°
Volume	1226.99(14) Å^3	
Z	2	
Density (calculated)	1.233 mg/m^3	
Absorption coefficient	0.034 mm^{-1}	
F(000)	480	
Crystal size	0.10 × 0.03 × 0.02 mm^3	
Theta range for data collection	0.970 to 15.342°	
Index ranges	$-6 \le h \le 6$, $-12 \le k \le 12$, $-31 \le l \le 31$	
Reflections collected	34432	
Independent reflections	5118 [R(int) = 0.0612]	
Completeness to thet a = 14.357°	94.70%	
Absorption correction	Semiempirical from equivalents	
Max. and min. transmission	0.7439 and 0.6349	
Refinement method	Full-matrix least-squares on F2	
Data/restraints/ parameters	5118/0/316	
Goodness-of-fit on F2	1.056	
Final R indices [I > 2σ(I)]	R1 = 0.0658, wR2 = 0.1501	
R indices (all data)	R1 = 0.0810, wR2 = 0.1589	
Extinction coefficient	n/a	
Largest diff. peak and hole	0.663 and −0.275 e.Å^{-3}	

https://doi.org/10.1021/acs.cgd.3c00002
Cryst. Growth Des. 2023, 23, 4164−4179

Scheme 3. Molecular Packing Showing Bifurcated Hydrogen Bonding by O(1) and C···C Close Contacts

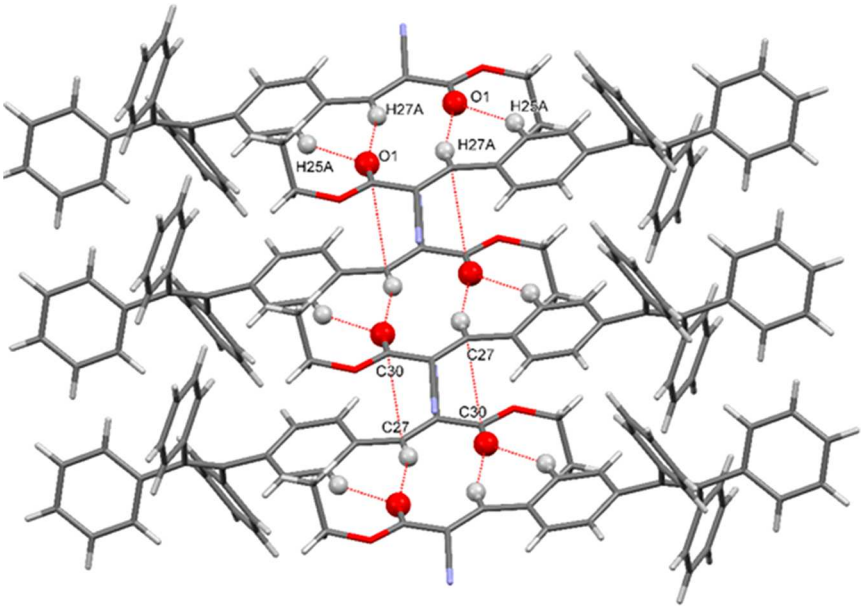

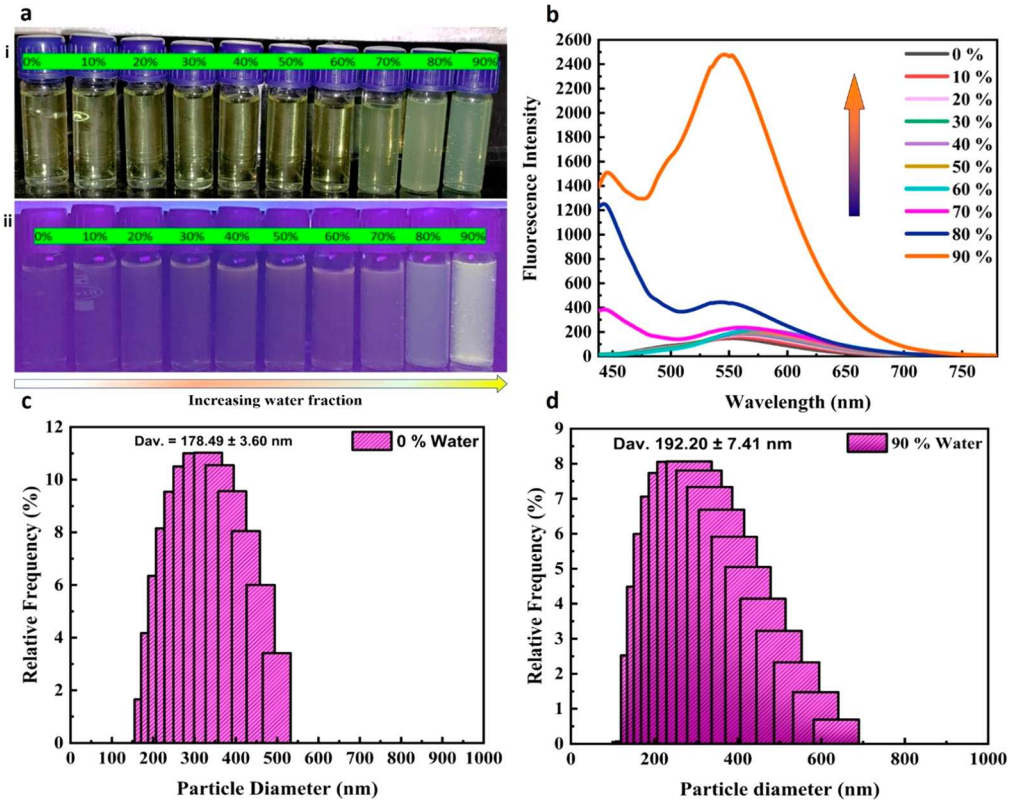

Figure 1. Photographic images of AIE in THF:H_2O mixtures with different water fractions (0−90%) − [a] (i) Under daylight and (ii) under UV (365 nm) irradiation. [b] Emission spectra (PL) of luminogen (TPE-SKJ) with different water fractions from 0% to 90% (THF/H_2O (v/v) mixtures recorded at $\lambda_{ex.}$ = 417 nm). The DLS measurements with (c) 0% water and (d) 90% water.

C−H···O intra- as well as intermolecular hydrogen bonding is observed in this compound. Intramolecular hydrogen bonding observed to C(32)−H(32C)···O(1) (d(D−H) = 0.98 Å, d(H···A) = 2.59, d(D···A) = 3.104(3) Å, ∠D−H···A = 113.1°) and the oxygen O(1) shows bifurcated intermolecular hydrogen bonding to H(25A) (d(D−H) = 0.950 Å, d(H···A) = 2.496 Å, d(D···A) = 3.368(3) Å, ∠D−H···A = 152.6°, 2-x,1-y,1-z) and H(27A) (d(D−H) = 0.950 Å, d(H···A) = 2.407 Å, d(D···A) = 3.316(3) Å, ∠D−H···A = 160.3°, 2-x,1-y,1-z) of the neighboring molecules to form a hydrogen-bonded dimer. The hydrogen-bonded dimers are in close contact via C(27)···C(30) (3.249 Å, 1-x,1-y,1-z) (Scheme 3).

3.3. Photophysical Properties. *3.3.1. AIE Characteristics of TPE-SKJ.* Aggregation-induced emission (AIE), a noteworthy photophysical phenomenon, was reported by B. Z. Tang and his colleagues in 2001. It is directly linked to the

https://doi.org/10.1021/acs.cgd.3c00002
Cryst. Growth Des. 2023, 23, 4164−4179

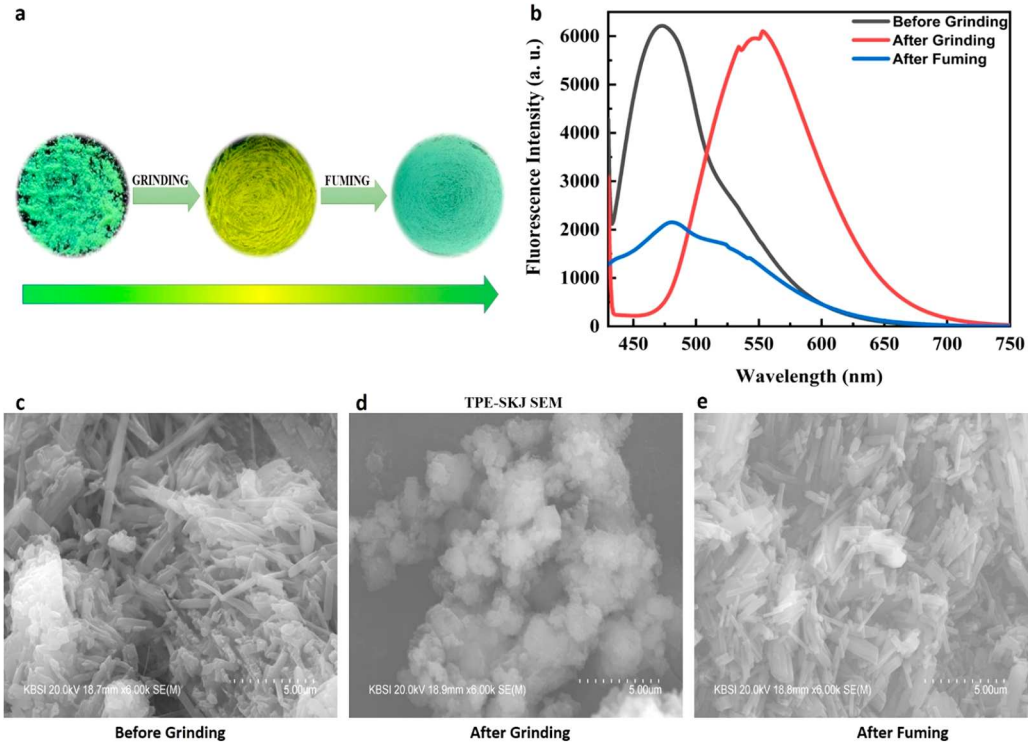

Figure 2. (a) Photographs of mechanochromic properties under UV irradiation (365 nm) before grinding, after grinding, and after fuming with organic solvent (acetone). (b) The PL emission spectra of luminogen (TPE-SKJ): before grinding, after grinding, and after fuming with acetone. FE-SEM images of TPE-SKJ (c) before grinding, (d) after grinding, and (e) after fuming, respectively.

aggregation of luminogens and their fluorescence emission in an aggregate (solid) state.[39−41] In the aggregation-induced emission process, the nonemissive or weakly emissive luminogens are converted into highly emissive because of the aggregate formation of the luminogens after increasing the fractions of water, which depends on the water quantity in the mixture. Such types of remarkable fluorescent luminogens or AIEgens have been widely used in diverse fields.[33,42]

Accordingly, to verify the (AIE phenomenon, we have performed this activity by using THF (tetrahydrofuran) and water. The photographic images under daylight and UV light are depicted in (Figure 1a). With the increase in the water quantity (0 to 90%), these images showed the AIE phenomenon in the synthesized luminogen. There is a significant increase in the fluorescence observed naked eye (Figure 1a-i) as well as under UV irradiation 365 nm (Figure 1a-ii). Moreover, to confirm AIE activity spectroscopically, we have studied the fluorescence emission behavior of luminogen-containing tetrahydrofuran solution with different (increasing) proportions of water fractions from f_w = 0% to 90%, as shown in (Figure 1b). The synthesized luminogen (TPE-SKJ) displayed an almost negligible (zero) emission in the tetrahydrofuran solution (Figure 1b) upon excitation at λ_{ex} = 417 nm. A small change in the emission was observed at 70% and 80% water fractions. However, a sudden increase in the emission was observed at 90/10% of H_2O/THF concentration at 550 nm, because of the formation of an aggregation of TPE-SKJ in water.[43−45]

These data indicate the synthesized novel luminogen exhibits excellent aggregation-induced emission (AIE) characteristics, and it shows the highest fluorescence intensity at f_w = 90% in THF/H_2O, according to the previous reports.[33] The DLS data demonstrates how the TPE-SKJ enhanced the size distribution with just an increase in water fraction from 0% to 90%. At 0% water fraction, the particle size was found to be 178.49 ± 3.60 nm (Figure 1c), whereas the particle size increased to 192.20 ± 7.41 nm at 90% water fraction (Figure 1d).

3.3.2. Mechanochromic Luminescent Behavior of TPE-SKJ. Mechanochromic luminescence (MC property) is an extraordinary photophysical phenomenon of some intelligent materials and molecules that responds to mechanical forces, including grinding and crushing/rubbing.[46] Due to its potential applications in security documents, mechanosensory devices, and optical storage, mechanochromic luminous properties have received significantly greater attention in recent years.[47] To check the mechanochromic response of the synthesized luminogen (TPE-SKJ); initially, it was ground in a mortar and pestle. Accordingly, Figure 2a shows the color of TPE-SKJ under UV light (365 nm). The as-synthesized TPE-SKJ shows green color; the yellow color formed after grinding and reverts to a faint green after fuming. When the solid sample of luminogen was ground with a mortar and pestle, the original green emission was dramatically switched to a yellow emission. Furthermore, fuming with the solvent's (acetone) vapor impacted the solid-state color of luminogen. After being vaporized with acetone, the luminogens color changes from yellow to its original color but shows faint green.[48,49]

Numerous cyano-substituted fluorogenic derivatives of tetraphenylethene have recently been discovered. They exhibit a variety of stimuli-responsive fluorescence transitions in the solid state, including piezo chromic, mechanochromic, vapochromic, hypochromic, and thermochromic fluorescence transitions.[50,51] This implies that they can alter their fluorescence characteristics in response to external factors such as pressure, volatiles, and temperature. The TPE-SKJ is a

https://doi.org/10.1021/acs.cgd.3c00002
Cryst. Growth Des. 2023, 23, 4164−4179

mechanochromic active material because it contains both cyano groups and TPE moieties. The solid green TPE-SKJ produces bright green emissions. The TPE-SKJ solid turns a pale yellow during 2 to 3 min of mortar and pestle grinding. The as-prepared solid of TPE-SKJ with a light green powder can be made by simply fuming with acetone.[52]

To confirm this interesting mechanochromic phenomenon, we have studied the fluorescence emission behavior and recorded the field emission scanning electron microscopy images of the TPE-KSJ before grinding, after grinding, and eventually fuming with acetone, as shown in Figure 2. In the PL spectra of the as-prepared (before grinding) TPE-SKJ, the emission peak was observed at 473 nm, while the emission peaks after grinding were observed at 553 nm (Figure 2b). This demonstrates that the grinding process caused an 80 nm spectral redshift, a typical mechanochromic exhibition. In the subsequent measurement, the grounded solid material was fumigated with acetone. It returns to its initial state and shows the same kind of PL emission but with low intensity (Figure 2b).[33,47]

The obtained mechanochromic properties of luminogen (TPE-SKJ) were further studied by powder X-ray diffraction (PXRD) patterns. The PXRD pattern was taken before grinding (as synthesized), which was scanned from 2θ of 5−80° (Figure 3-I). This pattern shows several sharp peaks

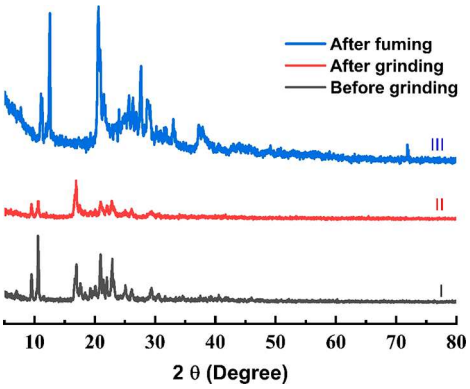

Figure 3. Mechanochromic XRD patterns in various solid states [(I) before grinding (II), after grinding, and (III) after fuming].

(between 2θ = 9.5−30°) The as prepared sample (before grinding) shows XRD peaks at 2θ = 9.47°, 10.69°, 16.95°, 17.76°, 20.99°, 22°, 22.81°, 25.04°, 26.25°, 29.28°, and 30.69°.[33]

After grinding, the synthesized luminogen shows altered peak intensity order. Except for the peak at 17°, other peaks become less intense after grinding, while after grinding it shows XRD peaks at 9.46°, 10.59°, 16.86°, 17.48°, 20.92°, 21.93°, 22.94°, 25.16°, 26.17°, and 29.40°. The XRD peak intensity decreased for sample II because of its amorphous nature (Figure 3-II). This led to the change in the orthorhombic crystal structure which is responsible for the shifting of the emission peak from 473 to 545 nm in PL spectra (Figure 2b), and it also supports the change in color after grinding the compound from green to yellow (Figure 2a).

To check the reverse phenomena of TPE-SKJ, it was subjected to a fuming process. Therefore, the PXRD pattern was recorded after fuming with acetone; the after fuming sample shows peak at 11.20°, 12.60°, 20.56°, 21.52°, 23.88°, 25.50°, 26.31°, 27.52°, 28.74°, 30.35°, 31.77°, 33.18°, 37.22°, 38.03°, and 71.89°. The after fuming XRD peak shifts might be due to the change in the lattice parameters and high crystallinity, a slightly broad signature of diffraction peaks in the pattern than its previous states (as-prepared and after grinding processes). The peak positions revealed that it reverts with higher intense peaks entirely to its original crystalline state after fuming (Figure 3-III). However, we got some extra peaks at around 33°, 38°, and 72° which might be coming from the presence of acetone.[53] Moreover, the reversible mechanochromic observation was further strongly confirmed by PL emission spectra (Figure 2b) where the emission peak was shifted back to a lower λ_{max} value (479 nm). Hence, the transformation from crystalline to semicrystalline phases of luminogen (TPE-SKJ) after fuming was accountable for its mechanochromic luminescence phenomenon.

This can be visualized from the field emission scanning electron microscope (FESEM) images also, where we got the aggregated needle-like morphology of the synthesized compound before grinding (Figure 2c). After grinding, the morphology of the TPE-SKJ luminogen was found to be aggregated spherical-shaped microparticles (Figure 2d).[54] After fuming, the surface area again increases indicating the decrease in its particle size which is due to the compound reverting to its original state, and it is further clearly visualized from the FESEM images, where the spherical shape converted back to needle-like morphology (Figure 2e).[55−57]

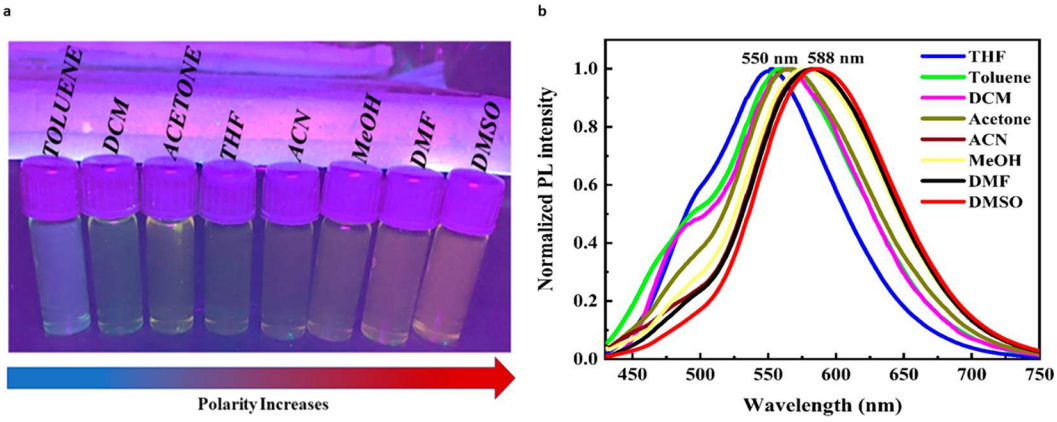

Figure 4. (a) Photographic image of solvatochromism with different solvents under UV irradiation (365 nm). (b) Normalized PL intensity emission spectra in the presence of different solvents.

https://doi.org/10.1021/acs.cgd.3c00002
Cryst. Growth Des. 2023, 23, 4164−4179

After recrystallization, the lattice parameters might be changed due to the fuming with acetone, and the increased peak intensity reflects the crystalline nature of III.

3.3.3. Solvatochromic Effect. The terms bathochromic shift, red shift, or positive solvatochromism are used for describing a shift of an absorption peak toward a longer wavelength. Such a change is noticeable when the $\pi-\pi^*$ transition occurs as we increase polarity. The energy level of an excited and unexcited state is reduced due to an increasing interaction between the solvent and the absorbing species. However, the effect is more noticeable in an excited state. Solvent polarity both influences and has the potential to change the transitions. When in the granular state, polar solvents stabilize the former more than the latter. As a result, as the solvent polarity increases, a bathochromic change arises.

As we know, with increasing solvent polarity, the $\pi-\pi^*$ transition of polar compounds is encouraged to a longer wavelength and, usually, toward higher intensity. Since the excited state in this transition is more polar than the ground state, the bathochromic shift results from the dipole−dipole interaction with a polar solvent decreasing the energy of the excited state more than the ground state.[58]

The change in the color of luminogen in the presence of different solvents is commonly known as solvatochromism. The solvatochromic investigation of the synthesized luminogen (TPE-SKJ) was carried out by recording emission spectra in the presence of other polar solvents. The photographic images under UV irradiation (365 nm) are depicted in Figure 4a. In toluene, the luminogen shows strong blue fluorescence with an emission peak at 550 nm (Figure 4b). With the solvents' increasing polarity, a continuous bathochromic shift (blue to red) was observed. In the case of the highest polar solvent (DMSO), the emission spectrum was observed at 588 nm, and 38 nm bathochromic shifts were observed (Figure 4b). According to experimental results, the synthetic luminogen (TPE-SKJ) exhibits strong solvatochromic performance. As shown in Figure 4a,b, when the solvent is switched from nonpolar (such as toluene) to highly polar (DMSO), the PE-SKJ exhibits an apparent red shift from 550 to 588 nm. Figure 4a shows the fluorescence pictures of the respective solutions, which were captured using different solvents under UV irradiation (365 nm). The TPE-SKJ luminogen emits a potent blue light in toluene when exposed to UV light, and the shades of redshift get darker as they get closer to dimethyl sulfoxide (DMSO). Additionally, the change in solvent polarity results in a significant red shift from 550 to 588 nm.[47]

3.4. Analytical Studies of TPE-SKJ. *3.4.1. Fluorescence Response of Luminogen for Various Anions.* The anion recognition property of synthesized luminogen (TPE-SKJ) was investigated by using the fluorescence spectroscopic method. The solution of 1×10^{-4} M luminogen in acetonitrile was studied in the presence of various environmentally and biologically essential anions such as SO_4^{-2}, BrO_3^-, S^{-2}, $Cr_2O_7^{-2}$, HPO_4^{-2}, IO_3^-, MnO_4^-, SO_3^{-2}, SCN^-, CO_3^{-2}, CrO_4^-, I^-, etc., in aqueous media. As we have used a few salts as sensing performers, the type of cation is fundamental and significant information for anion sensing performance. The anions of Na and K containing salt have been used for the analytical studies of TPE-SKJ. The only anions that interact with cations are those that belong to group 1 and are the type 1 cation. The maximum emission peak was observed at 555 nm when the luminogen suspension was excited by using a 417 nm wavelength. The addition of a 100 μgmL^{-1} concentration solution of various anions to the AIEgen (TPE-SKJ) solution caused variations in the fluorescence emission spectra of luminogen. However, the fluorescence spectrum of probe 1 showed significant and drastic quenching in fluorescence in the presence of a MnO_4^- anion, indicating that probe 1 is selectively and sensitively suitable for the detection of MnO_4^- ion in the mixed aqueous media, as shown in Figure 5. Other

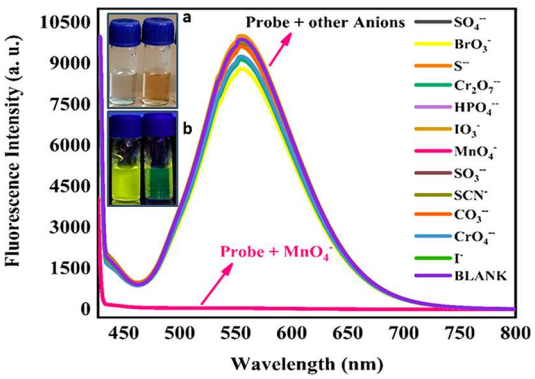

Figure 5. Fluorescence emission spectra (PL) of luminogen (TPE-SKJ) upon excitation and addition of different anions in aqueous media (inset: photographic image of TPE-SKJ with absent and present of MnO_4^- [a] under ambient light and [b] under UV irradiation).

anions do not change their fluorescence intensity drastically. The fluorescence intensity was negligible compared to the MnO_4^- ion. Interestingly, the concentration of all the anions is the same; still, the MnO_4^- ion flattens the curve compared to the rest of the anions. This reveals that MnO_4^- ion has much more affinity than other tested anions.

The changes in fluorescence were also recorded under ambient and UV irradiation at 365 nm, as shown in Figure 6a and b, respectively. Under ambient light, luminogen in mixed aqueous media (1:9, acetonitrile:water) shows a yellowish color to the MnO_4^- ion, and transparent color was observed for other anions (Figure 6a). In the case of UV light irradiation, all anions possess excellent fluorescence with yellow color, owing to the AIE. On the other hand, MnO_4^- ion-containing tubes only show faint blue color (Figure 6b). The plausible mechanism behind the sensing of MnO_4^- is highlighted in Scheme 4.

The completely remarkably diminished fluorescence (PL emission) of luminogen solution containing MnO_4^- ion shows due to the interaction between luminogen and MnO_4^- ions. However, other ions may not interact with luminogen; hence there is no appreciable change in fluorescence. These findings suggest that luminogen (TPE-KSJ) can selectively and sensitively detect the MnO_4^- ion over the most relevant anion. As a result, luminogen can be used as a fluorescent sensor to detect of MnO_4^- ions.

3.4.2. UV−vis Absorption Study of TPE-SKJ with Various Anions. In a mixed solution of acetonitrile and water (ACN:H_2O 1:9 v/v), the UV−vis spectra of synthesized luminogen (TPE-SKJ) were recorded at room temperature and shown in (Figure 7). The absorption peak of the luminogens is concentrated at a wavelength of 400 nm. The UV−vis absorption of luminogen did not significantly change with the addition of all the tested anions, excluding the MnO_4^- ion. The MnO_4^- ion ultimately affected the absorption spectra. The absorption maximum at 400 nm disappeared, and a new curve

https://doi.org/10.1021/acs.cgd.3c00002
Cryst. Growth Des. 2023, 23, 4164−4179

Figure 6. Photographs of luminogen (TPE-SKJ) with different anions (a) under ambient (day) light and (b) under UV irradiation (365 nm).

Scheme 4. Schematic Representation of AIE and Plausible Binding Mechanism of TPE-SKJ with MnO_4^-

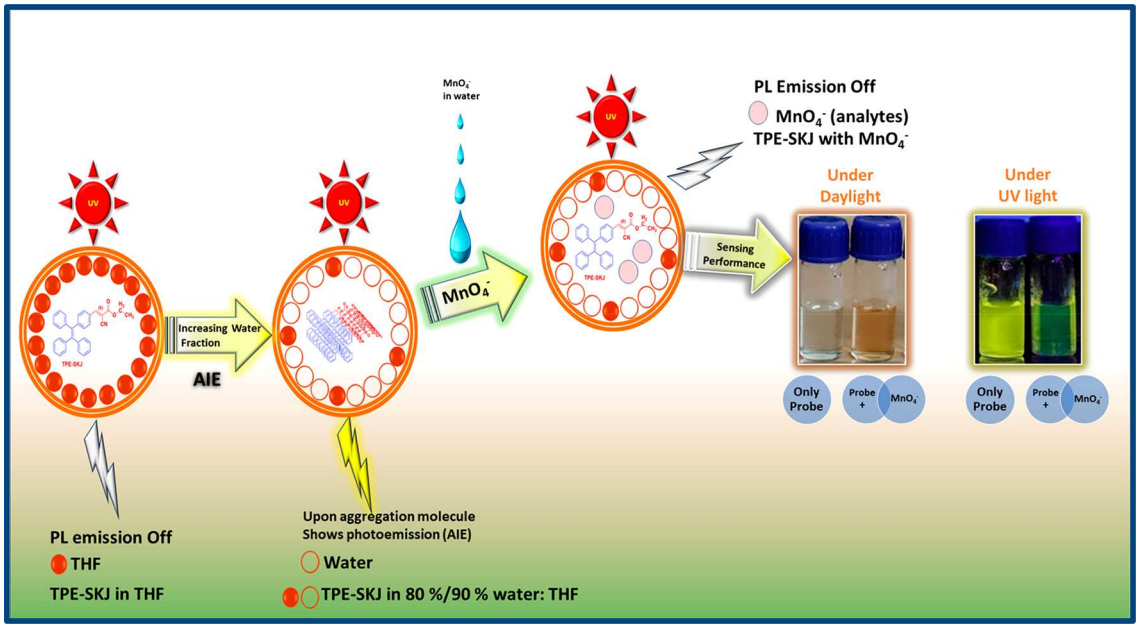

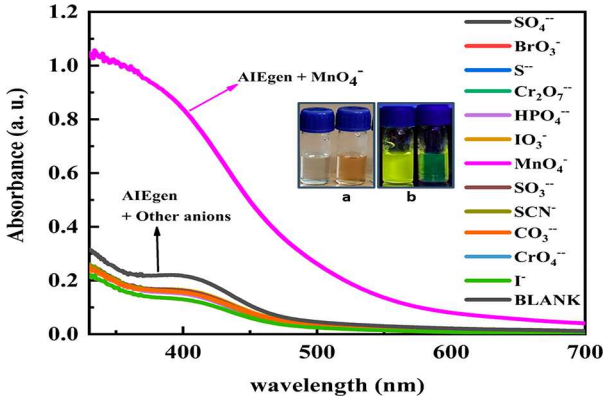

Figure 7. UV−vis spectra of the luminogen (TPE-SKJ) in the absence and presence of MnO_4^- over other anions. Inset: Photographic image of TPE-SKJ in the absence and presence of MnO_4^- [a] under ambient light and [b] under UV irradiation.

appeared at 390 nm with a blue shift by 10 nm. The luminogen complex formation with MnO_4^- ions may have been responsible for the differences in UV−vis absorption spectra. The coordination of MnO_4^- to the organic moiety may be responsible for forming the new absorption band at 390 nm.

3.4.3. Selectivity Study of Luminogen (TPE-SKJ) for MnO_4^-. For evaluating the selectivity of TPE-SKJ luminogen for detection of MnO_4^-, we investigated the emission characteristics of the TPE-SKJ with the presence of various other competitors of MnO_4^- anions such as SO_4^{-2}, BrO_3^-, S^{-2}, $Cr_2O_7^{-2}$, HPO_4^{-2}, IO_3^-, MnO_4^-, SO_3^{-2}, SCN^-, CO_3^{-2}, CrO_4^-, and I^- in a 9:1 (v/v) ACN:water mixture at room temperature. The TPE-SKJ luminogen did not show a remarkable and considerable response to the different competitors to MnO_4^-, as shown in Figure 8d. These results clearly show the selective detection of MnO_4^- over other pollutants (anions).

3.4.4. Fluorescence Sensing Performance of TPE-SKJ. The MnO_4^- ion sensing ability of synthesized luminogen (TPE-SKJ) in mixed aqueous conditions (acetonitrile:water v/v 1:9) was investigated in this section. The spectral findings can be seen in (Figure 5). After 417 nm excitation, probe 1 in acetonitrile displayed the fluorescence emission band at 555 nm with the addition of various concentrations of MnO_4^- ions

https://doi.org/10.1021/acs.cgd.3c00002
Cryst. Growth Des. 2023, 23, 4164−4179

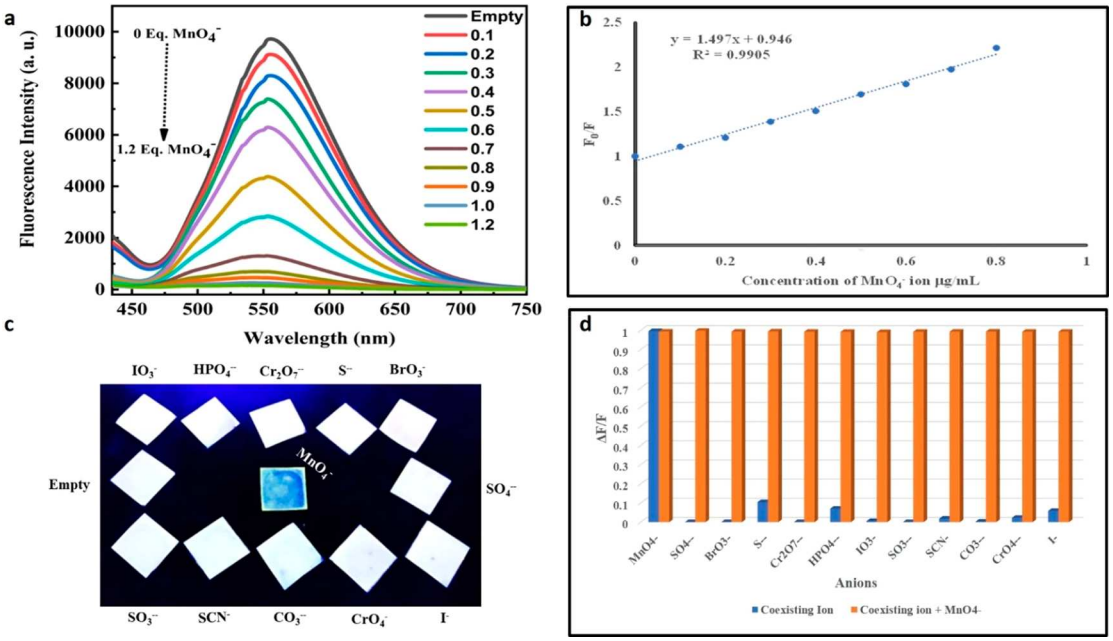

Figure 8. (a) MnO_4^- in an aqueous salt solution was added in different concentrations from 0 to 1 μg mL^{-1} to the AIEgen (TPE-SKJ) solutions. (b) The Stern−Volmer plot between the F_0/F (relative PL intensity) vs different concentrations of MnO_4^-. (c) Photographic images of paper strips that are loaded with the luminogen (TPE-SKJ) as well as tested with other anions including MnO_4^- under UV irradiation (365 nm). (d) Bar diagram showing selectivity study of TPE-SKJ. The fluorescence intensity response $[\Delta F/F]$ of luminogen is plotted in the presence and absence of the MnO_4^- ion and several coexisting anions.

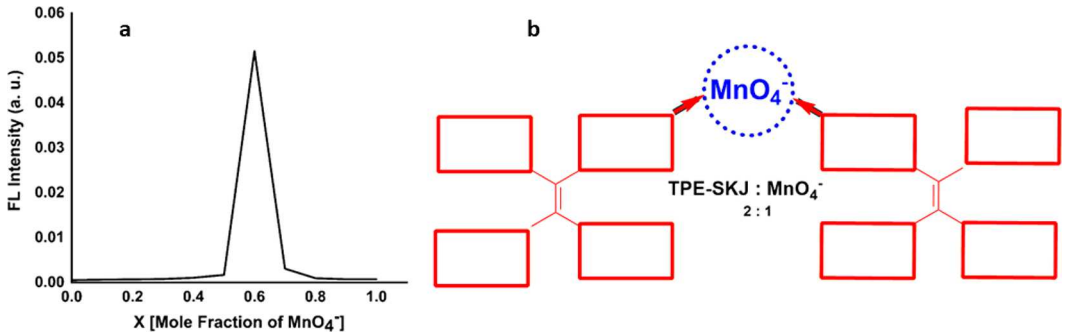

Figure 9. (a) The Job's plot showing 2:1 binding of TPE-SKJ with MnO_4^-. (b) Schematic representation of binding between TPE-SKJ and MnO_4^-.

in the probe 1 solution, and variations in the emission band at 555 nm were observed. The fluorescence of the probe 1 solution progressively decreases with the addition of MnO_4^- ions (0.1−1.6 μgmL^{-1}) and almost totally disappears after the addition of 1.6 μgmL^{-1} of both ions, as shown in (Figure 8a). Therefore, the results suggested that the organic probe can be used to determine the qualitative and quantitative amounts of MnO_4^- ions.

3.4.5. Stern−Volmer Plot. There should be a linear relationship between analyte concentration and signal intensity to establish an analytical method for quantifying analytes. Therefore, a standard Stern−Volmer quenching relationship was used in the present case to evaluate the analytical, linear range (Figure 8b).

$$F_0/F = 1 + K_{sv}[Q] \quad (1)$$

where [Q] is the ion concentration, K_{sv} is the Stern−Volmer constant, and F_0 and F are the fluorescence intensities in the absence and presence of MnO_4^- ion, respectively. The plot of F_0/F against ion concentration shows the linear relationship between fluorescence response and their concentration throughout the range of (0 to 1.2 × μg mL^{-1}), as shown in Figure 8b. Furthermore, all data points are present on the fitted line (R^2 = 0.9905), suggesting a good linear relationship between fluorescence response and concentration.

3.4.6. Limit of Detection (LOD). The limit of detection (LOD) of the developed method was subsequently evaluated by using the following equation

$$\text{Detection limit} = 3\sigma/K \quad (2)$$

where s is the standard deviation of the blank measurement and K is the slope of the plot between the ratio of emission intensity vs luminogen. The Stern−Volmer plot has been used to calculate the LOD of the developed sensing system. The LOD of the present case was found to be 0.086009 μgmL^{-1} for the MnO_4^- anion. The permissible limit of MnO_4^- ions in drinking water is much higher than the present LOD. The linearity, correlation coefficient, and LOD indicate that the current sensing system is fairly accurate and can be used to determine the MnO_4^- ions in actual samples.[59]

https://doi.org/10.1021/acs.cgd.3c00002
Cryst. Growth Des. 2023, 23, 4164−4179

Scheme 5. Overall Graphical Representation of the AIE Study with Applications of the Luminogen (TPE-SKJ)

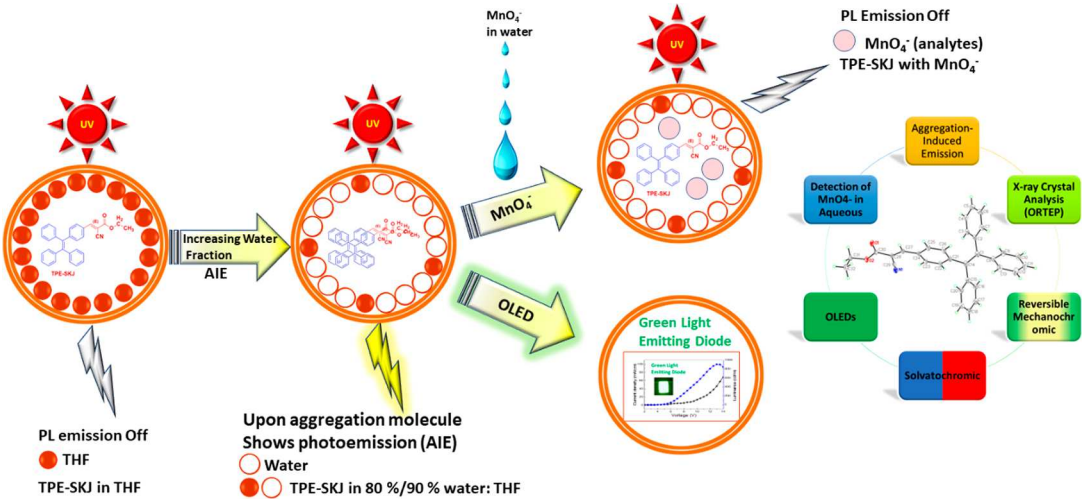

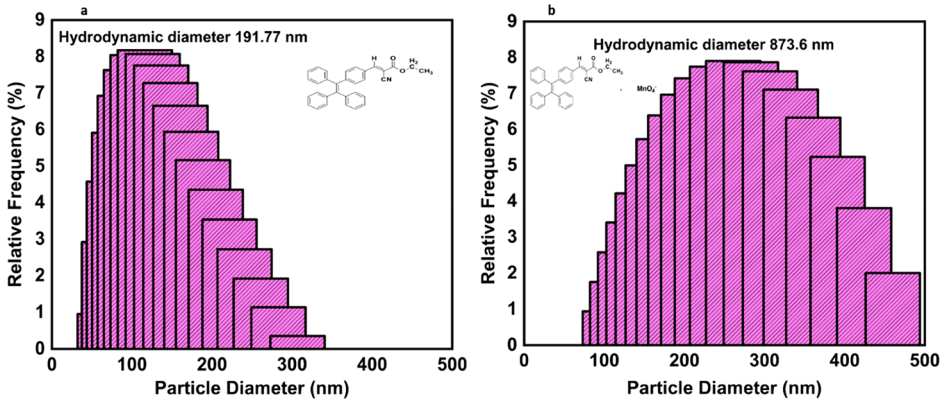

Figure 10. DLS results of TPE-SKJ in the (a) absence and (b) presence of MnO_4^- ions.

3.4.7. Onsite Detection of MnO_4^- by Paper-Based Strips of TPE-SKJ. Visual detection is the easiest way to explore the different pollutants. In the present case, a paper strip was used to detect the MnO_4^- ions. The paper strips were dipped in an acetonitrile solution of luminogen (TPE-SKJ) and dried in the open air. To detect MnO_4^-, UV light (365 nm) was used. Under UV light, it was noticed that the luminogens on a blank test paper fluoresced normally (Figure 8c). After the MnO_4^- anion was added to the paper strip containing luminogen, the test paper strip was fluorescence and showed a deep blue color (Figure 8c). On the other hand, the competing anions had no impact and did not show any considerable fluorescence. These results indicate that the synthesized luminogen has excellent selectivity, sensitivity, and rapidity, requires less instrumentation, and has operational simplicity for visual detection of MnO_4^- anion.[33]

3.4.8. Job's Plot. The Job's plot (FL intensity vs mole fraction of MnO_4^-) established the stoichiometry of binding between the TPE-SKJ with MnO_4^- and it was found to be 2:1, as shown in Figure 9a. The binding between the TPE-SKJ and MnO_4^- is schematically shown in (Figure 9b).[5]

3.4.9. Quantum Yield. The probes' fluorescence quantum yield (Φ_F) in the absence of MnO_4^- anion was calculated using the quinine sulfate ($\Phi_F = 0.54$) as a reference. The value of Φ_F was determined using the following eq 3.

$$\Phi_F = \Phi_{ref} \times I_{probe}/I_{ref} \times A_{ref}/A_{probe} \times {\eta_{probe}}^2/{\eta_{ref}}^2 \quad (3)$$

where Φ_F and Φ_{ref} are the probe's and quinine sulfate's quantum yields, respectively. The integrated emission peak regions of the probes and quinine sulfates are labeled as the I_{probe} and I_{ref}, respectively. The probe and quinine sulfate absorbance at the excitation wavelengths are denoted as A_{probe} and A_{ref}, respectively. The η_{probe} and η_{ref} are the solvents' respective refractive indices with 11% quantum yield, and the quantum yield of an aggregation states is 1.5%.[33,60]

4. SENSING MECHANISM OF TPE-SKJ

This work detected the MnO_4^- anions using the TPE-SKJ luminogen. The analysis of this detection was based on how MnO_4^- ions decreased the TPE-SKJ fluorescence intensity. The complexation of the TPE-SKJ with ions was thought to cause fluorescence quenching. The following techniques have been used to determine the sensing mechanism.

4.1. DLS Study. The particle size of TPE-SKJ was investigated both before and after the interaction of MnO_4^- with the help of the dynamic light scattering (DLS) measurement technique. The significant binding between the sensor TPE-SKJ and MnO_4^- was observed during the DLS measurements in an aqueous solution (9:1, v/v, water, and acetonitrile), and it exhibits a hydrodynamic diameter of 191.77 nm for TPE-SKJ in the absence of an anion, as shown in (Figure 10a). However, whenever MnO_4^- ions were added to the TPE-SKJ solution, the hydrodynamic diameter of TPE-SKJ increased significantly, reaching 873.60 nm (Figure 10b).

https://doi.org/10.1021/acs.cgd.3c00002
Cryst. Growth Des. 2023, 23, 4164−4179

This increase in hydrodynamic diameter is shown in (Figure 10b). The increase in the hydrodynamic diameter with the addition of an anion is clear evidence of the complex formation between TPE-SKJ and MnO_4^-. Thus, TPE-SKJ and the MnO_4^- anion easily form a complex.[33,61−63]

4.2. Fluorescence Lifetime. The time-correlated single-photon counting (TCSPC) was also used to confirm the exact mechanism behind the sensitive and selective MnO_4^- ion sensing in aqueous media over other anions by the TPE-SKJ luminogen. The emission of the luminogen with the MnO_4^- ions either the complex formation or the electron transfer mechanism might be primarily responsible for quenching the emission of luminogen with MnO_4^- ions. To differentiate such a quenching mechanism, the fluorescence lifetime measurement is an effective tool. The decay time of the luminogen with an increasing quantity (00, 0.1, 0.5, and 1 mL) of the MnO_4^- (1 μg mL^{-1}) solution was recorded with lifetime 00 mL = 1.867 ns, for 0.1 mL = 2.54 ns, for 0.5 mL = 636.17 ps, and 1.0 mL = 636.17 ps, respectively, and the results are depicted in (Figure 11).

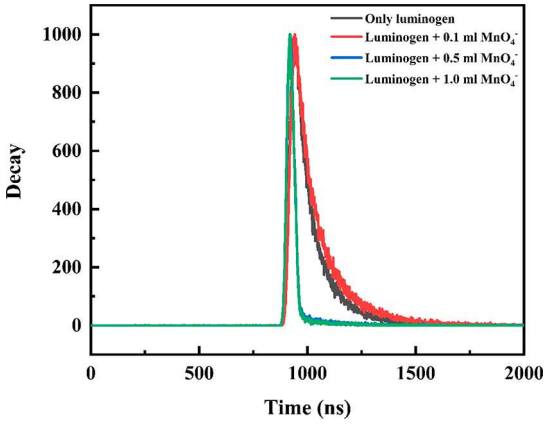

Figure 11. Fluorescence decay profile (lifetime) of luminogen (TPE-SKJ) in the presence and absence of a different concentration of anion (MnO_4^-) solution.

If $\tau_0/\tau = 1$, the type of quenching is static, and if $\tau_0/\tau = F_0/F$, the type of quenching is dynamic, where τ_0 and τ_1 are the lifetimes of the fluorophore (luminogen) before and after the quencher (MnO_4^-). The results suggested the $\tau_0/\tau = F_0/F$, which indicated that there is a dynamic form of quenching between the luminogen and MnO_4^- ions. As per the results, there is a complexation between the luminogen (TPE-SKJ) and anions at an excited state, as shown in Figure 11.[33]

4.3. Binding Sites and Binding Constant. To determine binding parameters such as the binding constant (K) and binding sites (n), fluorescence quenching data at 298 K were used. The following equation was used to calculate the binding parameters (eq 4).

$$\log[(F_0 - F)/F] = \log K + n\log[Q] \quad (4)$$

By plotting the $\log[(F_0 - F)/F]$ vs $\log[Q]$ at room temperature, we can obtain the values of K (binding constant) and n^a (binding sites), as shown in (Figure 12, Table 2). The regression coefficient, intercept, and slope were utilized to calculate the binding constant (K) and binding sites (n^a). The results of luminogen (TPE-SKJ) indicate that there is a single class of binding sites (n^a) with around 3 being the approximate number of binding sites (n^a).[33,60]

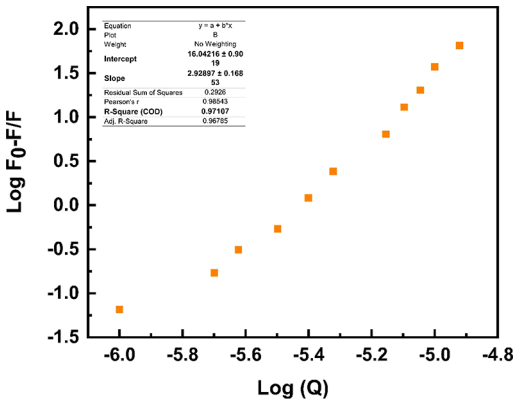

Figure 12. Plot of Log $F_0 - F/F$ against Log Q at room temperature.

Table 2. Binding Constant (K) and the Number of Binding Sites (n^a) between the Luminogen and MnO_4^- (Analyte)

Analyte	Correlation Coefficient (R)	Binding Constant K ($\times 10^6$ dm^3 mol^{-1})	Number of Binding Sites (n^a)
MnO_4^-	≈ 0.98	0.067	≈ 3.0

5. ELECTROLUMINESCENCE PROPERTIES (OLEDS) OF TPE-SKJ

The high photoluminescence (PL) efficiency and good thermal stability of synthesized luminogen (TPE-SKJ) inspire us to investigate its electroluminescence (EL) properties. Here, we have fabricated an organic light emitting device (OLED) with a structure of ITO/PEDOT:PSS (40 nm)/EML (70 nm)/TPBi (40 nm)/LiF (0.8 nm)/Al (120 nm), as shown in (Figure 13a). The ITO and LiF/Al in the mentioned configuration act as anode and cathode, respectively. The PEDOT:PSS is used as a hole transport layer, whereas TPBi acts as a hole blocking layer. The luminogen (TPE-SKJ) works as an emissive layer (EML). The energy level of the EML falls between the PEDOT:PSS and TPBi, as depicted in the band diagram of the fabricated device (Figure 13b). The smooth and homogeneous film formation is important for the optoelectronic performance of the device. Therefore, we analyzed the surface morphology of the emissive layer by atomic force microscopy. The root means square (RMS) roughness was found to be very small (0.38 nm), as indicated in (Figure 13c). These results exemplify that the solution-processed organic emissive layer is thermally stable, uniform, and adherent.[28]

The EL emission spectrum of the device peaked at 538 nm, almost identical with the PL emission that indicates confinement of the exciton recombination zone inside the light emitting layer (Figure 13d). The current density−voltage−luminescence characteristics are shown in (Figure 13e). The inset shows a favorable electron and hole injection-driven light-emitting device at 10 V (light emission image). External quantum efficiency as a function of luminescence is shown in (Figure 13f). The device exhibits a maximum of 1.62% external quantum efficiency (EQE), which is relatively high for nondoped EML-based OLEDs. The turn ON voltage of the device is 3.5 V, whereas 900 cd m^{-2} is the maximum luminescence of the device. These results demonstrate the great potential of TPE-SKJ as a light emitter for solution-processed OLEDs.[27,29]

https://doi.org/10.1021/acs.cgd.3c00002
Cryst. Growth Des. 2023, 23, 4164−4179

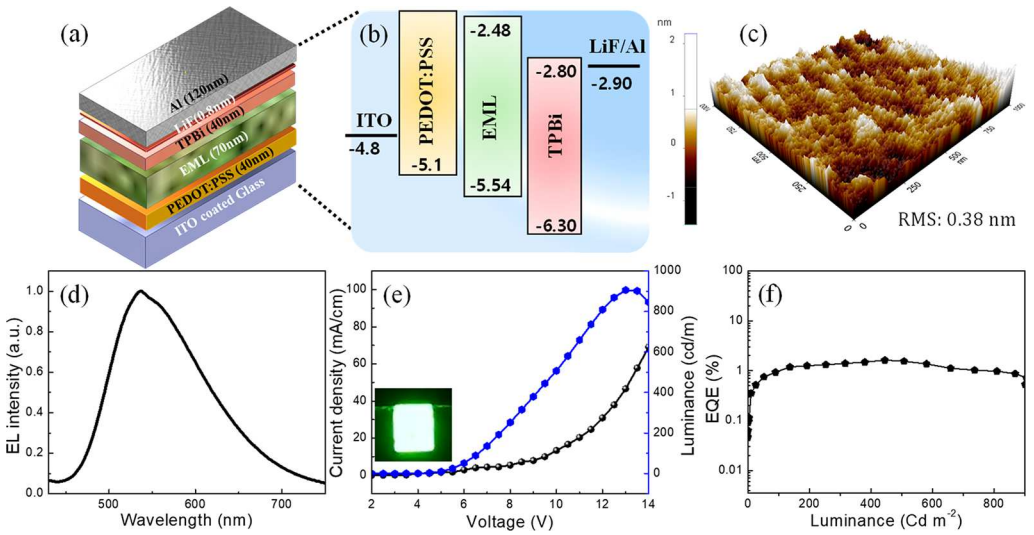

Figure 13. (a) Schematic of TPE-SKJ-based OLED. (b) Energy band diagram of the fabricated device. (c) AFM image of the emissive layer. (d) Experimentally obtained PL spectra at a fixed current density of 1 mA cm^{-2}. (e) Current density-luminance-driving voltage characteristics. The inset shows an emission image captured at 10 V. (f) EQE vs luminance characteristics of the device.

6. CONCLUSION

In conclusion, a novel tetraphenylethene-based AIEgen coded as TPE-SKJ was synthesized using the Suzuki-coupling reaction, confirmed by the different spectroscopic techniques and single crystal study. The synthesized TPE-SKJ exhibits a green color when exposed to UV radiation (365 nm) and exhibits various photophysical phenomena including aggregation-induced emission, reversible mechanochromism, and solvatochromism. The experiments with the MnO_4^- ions demonstrate the selectivity with which TPE-SKJ can detect MnO_4^- over the other anions in aqueous media. The S−V calculations show that the TPE-SKJ has the lowest detection limit with a value of 0.086009 μgmL^{-1} and a quantum yield (Φ) of 11%. Paper strip-based sensing has also been utilized for the on-site detection of MnO_4^- in actual samples. The DLS technique, fluorescence lifetime measurements, and calculations of the binding sites and binding constant studied the sensing mechanism. The outcomes of the present work support the potential use of TPE-SKJ for detecting MnO_4^- contaminants. Furthermore, we added TPE-SKJ to the organic light-emitting diode as an emissive layer. The device has a maximum EQE of 1.62%, higher than nondoped EML-based OLEDs emitting green light. The results of the present investigation suggested that the TPE-SKJ is a novel stimuli-responsive organic luminogen having single crystal study with different photophysical properties, which can be exploited for numerous sensing and optoelectronic applications.

■ ASSOCIATED CONTENT

Supporting Information

The Supporting Information is available free of charge at https://pubs.acs.org/doi/10.1021/acs.cgd.3c00002.

Scheme 1: Synthetic route of TPE-SKJ [(*E*)-ethyl 2-cyano-3-(4-(1,2,2-triphenylvinyl) phenyl) acrylate (*E*)-ethyl 2-cyanobut-2-enoate]. Scheme S2: Molecular structure of TPE-SKJ in 3D (Color code: Carbon: Silver, Hydrogen: Purple, Oxygen: Red, Nitrogen: Blue). Tables S1 to S5: Representative crystallographic data. Figure S1: IR Spectrum of (*E*)-ethyl 2-cyano-3-(4-(1,2,2-triphenylvinyl) phenyl) acrylate. Figure S2: ^{1}H NMR Spectrum of (*E*)-ethyl 2-cyano-3-(4-(1,2,2-triphenylvinyl) phenyl) acrylate. Figure S3: ^{13}C NMR Spectrum of (*E*)-ethyl 2-cyano-3-(4-(1,2,2-triphenylvinyl) phenyl) acrylate. Figure S4: ^{13}C DEPT-135 NMR Spectrum of (*E*)-ethyl 2-cyano-3-(4-(1,2,2-triphenylvinyl) phenyl) acrylate. Figure S5: HRMS Spectrometry of (*E*)-ethyl 2-cyano-3-(4-(1,2,2-triphenylvinyl) phenyl) acrylate. Figure S6: Shows an AFM analysis and AFM topographic analysis of the EML layer. Figure S7: Representing (a) IV Characteristics, (b) Current Density Dependent Luminescence, and (c) Voltage-Dependent External Quantum Efficiency Curve, respectively. (PDF)

Accession Codes

CCDC 2221617 contains the supplementary crystallographic data for this paper. These data can be obtained free of charge via www.ccdc.cam.ac.uk/data_request/cif, or by emailing data_request@ccdc.cam.ac.uk, or by contacting The Cambridge Crystallographic Data Centre, 12 Union Road, Cambridge CB2 1EZ, UK; fax: +44 1223 336033.

■ AUTHOR INFORMATION

Corresponding Author

Prashant V. Anbhule − *Medicinal Chemistry Research Laboratory, Department of Chemistry, Shivaji University, Kolhapur, Maharashtra 416004, India;* orcid.org/0000-0003-1681-6349; Phone: +91 231 260 9169; Email: pvanbhule@gmail.com; Fax: +91 231 2692333

Authors

Kishor S. Jagadhane − *Medicinal Chemistry Research Laboratory, Department of Chemistry, Shivaji University, Kolhapur, Maharashtra 416004, India;* orcid.org/0000-0003-3444-8586

Ray J. Butcher − *Department of Chemistry, Howard University, Washington, DC 20059, United States*

Tukaram D. Dongale − *Computational Electronics and Nanoscience Research Laboratory, School of Nanoscience and Biotechnology, Shivaji University, Kolhapur, Maharashtra 416 004, India*

https://doi.org/10.1021/acs.cgd.3c00002
Cryst. Growth Des. 2023, 23, 4164−4179

Kiran A. Nirmal − *School of Electrical Engineering, Korea University, Seoul 136-701, Republic of Korea*
Govind B. Kolekar − *Fluorescence Spectroscopy Research Laboratory, Department of Chemistry, Shivaji University, Kolhapur, Maharashtra 416004, India*
Mohaseen S. Tamboli − *Korea Institute of Energy Technology (KENTECH), Naju 58330 Jeollanam-do, Republic of Korea*
Tae Geun Kim − *School of Electrical Engineering, Korea University, Seoul 136-701, Republic of Korea;* orcid.org/0000-0001-6211-1134
Sunita Salunke-Gawali − *Department of Chemistry, Savitribai Phule Pune University, Pune, Maharashtra 411007, India;* orcid.org/0000-0002-4460-3992

Complete contact information is available at: https://pubs.acs.org/10.1021/acs.cgd.3c00002

Author Contributions

KSJ: Conceptualization, Ideas, Methodology, Synthetic route, Investigation, Experimental work, Characterization, Single Crystal grow, Photophysical phenomenon's, Sensing study, Writing - Original Draft, Writing - Review and Editing. RJB: Single Crystal analysis. TDD: Formal analysis. KAN: Methodology of OLED, Writing - Review and Editing. GBK: Writing - Review and Editing. MST: Review. TGK: Methodology of OLED, Writing - Review and Editing. SSG: Single Crystal analysis. PVA: Data Curation, Writing - Review and Editing, Visualization, and Supervision.

Funding

This work was financially supported by the Dr. Babasaheb Ambedkar Research and Training Institute (BARTI), Pune. (No. BARTI/Fellowship/BANRF-2018/19−20/3036).

Notes

The authors declare no competing financial interest.

■ ACKNOWLEDGMENTS

The authors (KSJ and PVA) are thankful to the Department of Chemistry, Shivaji University, Kolhapur for providing the all-research facility, and Sophisticated Analytical Instrument Facilities (SAIF) Centre, Shivaji University, Kolhapur for providing the required characterizations. The authors are also grateful for the financial support from the Dr. Babasaheb Ambedkar Research and Training Institute (BARTI), Pune. (No. BARTI/Fellowship/BANRF-2018/19-20/3036), and ChemMatCARS Sector 15 is supported by the National Science Foundation under grant number NSF/CHE-1834750. This research used resources of the Advanced Photon Source, a U.S. Department of Energy (DOE) Office of Science User Facility operated for the DOE Office of Science by Argonne National Laboratory under Contract No. DE-AC02-06CH11357.

■ REFERENCES

(1) Yang, J.; Fang, M.; Li, Z. Organic Luminescent Materials: The Concentration on Aggregates from Aggregation-induced Emission. *Aggregate* **2020**, *1* (1), 6−18.
(2) Li, Z.; Dong, Y. Q.; Lam, J. W. Y.; Sun, J.; Qin, A.; Häussler, M.; Dong, Y. P.; Sung, H. H. Y.; Williams, I. D.; Kwok, H. S.; Tang, B. Z. Functionalized Siloles: Versatile Synthesis, Aggregation-Induced Emission, and Sensory and Device Applications. *Adv. Funct. Mater.* **2009**, *19* (6), 905−917.
(3) Huang, J.; Sun, N.; Dong, Y.; Tang, R.; Lu, P.; Cai, P.; Li, Q.; Ma, D.; Qin, J.; Li, Z. Similar or Totally Different: The Control of Conjugation Degree through Minor Structural Modifications, and Deep-Blue Aggregation-Induced Emission Luminogens for Non-Doped OLEDs. *Adv. Funct. Mater.* **2013**, *23* (18), 2329−2337.
(4) Jagadhane, K. S.; Dongale, T. D.; Nikam, A. S.; Tadavalekar, N. B.; Kamat, R. K.; Kolekar, G. B.; Anbhule, P. V. Tetraphenylethene Carbothioamide-Based Organic Stimuli- Responsive Mechanochromic Memristive Devices with Non- Volatile Memory and Synaptic Learning Functionalities. *ChemistrySelect* **2023**, *8*, 9.
(5) Umar, S.; Jha, A. K.; Purohit, D.; Goel, A. A Tetraphenylethene-Naphthyridine-Based AIEgen TPEN with Dual Mechanochromic and Chemosensing Properties. *J. Org. Chem.* **2017**, *82* (9), 4766−4773.
(6) Liang, J.; Tang, B. Z.; Liu, B. Specific Light-up Bioprobes Based on AIEgen Conjugates. *Chem. Soc. Rev.* **2015**, *44* (10), 2798−2811.
(7) Xu, J.; Chi, Z. Mechanofluorochromism: An Overview. *Mechanochromic Fluorescent Materials* **2014**, No. 8, 1−6.
(8) Butler, T.; Morris, W. A.; Samonina-Kosicka, J.; Fraser, C. L. Mechanochromic Luminescence and Aggregation Induced Emission of Dinaphthoylmethane β-Diketones and Their Boronated Counterparts. *ACS Appl. Mater. Interfaces* **2016**, *8* (2), 1242−1251.
(9) Wang, J.; Mei, J.; Hu, R.; Sun, J. Z.; Qin, A.; Tang, B. Z. Click Synthesis, Aggregation-Induced Emission, E/Z Isomerization, Self-Organization, and Multiple Chromisms of Pure Stereoisomers of a Tetraphenylethene-Cored Luminogen. *J. Am. Chem. Soc.* **2012**, *134* (24), 9956−9966.
(10) Han, J.; Sun, J.; Li, Y.; Duan, Y.; Han, T. One-Pot Synthesis of a Mechanochromic AIE Luminogen: Implication for Rewritable Optical Data Storage. *J. Mater. Chem. C* **2016**, *4* (39), 9287−9293.
(11) Li, M.; Zhang, Q.; Wang, J. R.; Mei, X. Mechanochromism Triggered Fluorescent Color Switching among Polymorphs of a Natural Fluorescence Pigment. *Chem. Commun.* **2016**, *52* (75), 11288−11291.
(12) Mei, J.; Leung, N. L. C.; Kwok, R. T. K.; Lam, J. W. Y.; Tang, B. Z. Aggregation-Induced Emission: Together We Shine, United We Soar! *Chem. Rev.* **2015**, *115*, 11718−11940.
(13) Ding, D.; Li, K.; Liu, B.; Tang, B. Z. Bioprobes Based on AIE Fluorogens. *Acc. Chem. Res.* **2013**, *46* (11), 2441−2453.
(14) Hu, R.; Leung, N. L. C.; Tang, B. Z. AIE Macromolecules: Syntheses, Structures and Functionalities. *Chem. Soc. Rev.* **2014**, *43* (13), 4494−4562.
(15) Zhang, C.; Jin, S.; Yang, K.; Xue, X.; Li, Z.; Jiang, Y.; Chen, W. Q.; Dai, L.; Zou, G.; Liang, X. J. Cell Membrane Tracker Based on Restriction of Intramolecular Rotation. *ACS Appl. Mater. Interfaces* **2014**, *6* (12), 8971−8975.
(16) Zhao, Z.; Zhang, H.; Lam, J. W. Y.; Tang, B. Z. Aggregation-Induced Emission New Vistas at the Aggregate Level. *Angew. Chem. Int. Ed* **2020**, *59*, 9888.
(17) Chen, Y.; Lam, J. W. Y.; Kwok, R. T. K.; Liu, B.; Tang, B. Z. Aggregation-Induced Emission: Fundamental Understanding and Future Developments. *Mater. Horizons* **2019**, *6* (3), 428−433.
(18) Hong, Y.; Lam, J. W. Y.; Tang, B. Z. Aggregation-Induced Emission. *Chem. Soc. Rev.* **2011**, *40* (11), 5361−5388.
(19) Hong, Y.; Lam, J. W. Y.; Tang, B. Z. Aggregation-Induced Emission: Phenomenon, Mechanism and Applications. *Chemical Communications.* **2009**, 4332−4353.
(20) Sun, Z.; Sun, J.; Xi, L.; Xie, J.; Wang, X.; Ma, Y.; Li, L. Two Novel Lanthanide Metal-Organic Frameworks: Selective Luminescent Sensing for Nitrobenzene, Cu2+, and MnO_4^-. *Cryst. Growth Des.* **2020**, *20* (8), 5225−5234.
(21) Li, H.; Han, Y.; Shao, Z.; Li, N.; Huang, C.; Hou, H. Water-Stable Eu-MOF Fluorescent Sensors for Trivalent Metal Ions and Nitrobenzene. *Dalt. Trans.* **2017**, *46* (36), 12201−12208.
(22) Elavarasi, M.; Rajeshwari, A.; Alex, S. A.; Nanda Kumar, D.; Chandrasekaran, N.; Mukherjee, A. Simple Colorimetric Sensor for Cr(Iii) and Cr(vi) Speciation Using Silver Nanoparticles as a Probe. *Anal. Methods* **2014**, *6* (14), 5161−5167.
(23) Su, Y. Q.; Wang, R. T.; Blatova, O. A.; Shi, Y. S.; Cui, G. H. Two Robust Zn(Ii)-Organic Frameworks as Dual-Functional Fluorescent Probes for Efficient Sensing of Enrofloxacin and MnO_4−anions. *CrystEngComm* **2021**, *24* (1), 182−191.

(24) Huang, Y. W.; Chuang, P. M.; Wu, J. Y. Solvent-Induced Controllable Supramolecular Isomerism: Phase Transformation, CO2Adsorption, and Fluorescence Sensing toward CrO42-, Cr2O72-, MnO_4^-, and Fe3+. *Inorg. Chem.* **2020**, *59* (13), 9095−9107.
(25) Zhang, G. Q.; Gao, L. J.; Chai, H. M.; Ren, Y. X. Novel Multifunctional Samarium-Organic Framework for Fluorescence Sensing of Ag+, MnO_4^-, and Cimetidine and Electrochemical Sensing of o-Nitrophenol in Aqueous Solutions. *ACS Omega* **2021**, *6* (10), 6810−6816.
(26) Wang, L.; Tu, B.; Xu, W.; Fu, Y.; Zheng, Y. Uranyl Organic Framework as a Highly Selective and Sensitive Turn-on and Turn-off Luminescent Sensor for Dual Functional Detection Arginine and MnO_4^-. *Inorg. Chem.* **2020**, *59* (7), 5004−5017.
(27) Chen, L.; Zhang, C.; Lin, G.; Nie, H.; Luo, W.; Zhuang, Z.; Ding, S.; Hu, R.; Su, S. J.; Huang, F.; Qin, A.; Zhao, Z.; Tang, B. Z. Solution-Processable, Star-Shaped Bipolar Tetraphenylethene Derivatives for the Fabrication of Efficient Nondoped OLEDs. *J. Mater. Chem. C* **2016**, *4* (14), 2775−2783.
(28) Chen, L.; Lin, G.; Peng, H.; Nie, H.; Zhuang, Z.; Shen, P.; Ding, S.; Huang, D.; Hu, R.; Chen, S.; Huang, F.; Qin, A.; Zhao, Z.; Tang, B. Z. Dimesitylboryl-Functionalized Tetraphenylethene Derivatives: Efficient Solid-State Luminescent Materials with Enhanced Electron-Transporting Ability for Nondoped OLEDs. *J. Mater. Chem. C* **2016**, *4* (23), 5241−5247.
(29) Du, X.; Qi, J.; Zhang, Z.; Ma, D.; Wang, Z. Y. Efficient Non-Doped near Infrared Organic Light-Emitting Devices Based on Fluorophores with Aggregation-Induced Emission Enhancement. *Chem. Mater.* **2012**, *24* (11), 2178−2185.
(30) Awalekar, R.; Jagadhane, K.; Usmani, S.; Salunkhe, S.; Jamale, D.; Hangirgekar, S.; Kolekar, G.; Anbhule, P. Stereospecific Synthesis of (4E,10Z)-4,10-Tetradecadienyl Acetate, the Major Sex Pheromone of Apple Leaf Miner Moth, Phyllonorycter Ringoniella. *Lett. Org. Chem.* **2021**, *18* (8), 588−593.
(31) Jagadhane, K. S.; Bhosale, S. R.; Gunjal, D. B.; Nille, O. S.; Kolekar, G. B.; Kolekar, S. S.; Dongale, T. D.; Anbhule, P. V. Tetraphenylethene-Based Fluorescent Chemosensor with Mechanochromic and Aggregation-Induced Emission (AIE) Properties for the Selective and Sensitive Detection of Hg 2+ and Ag + Ions in Aqueous Media: Application to Environmental Analysis. *ACS Omega* **2022**, *7*, 34888.
(32) Jagadhane, K. S.; Bhosale, S. R.; Moyo, A. A.; Kolekar, G. B.; Sharma, K. K.; Yadav, H. M.; Anbhule, P. V. A Tetraphenylethene-Based Aggregation-Induced Emission Luminogen (AIEgen) With Mechanochromic Phenomena for Highly Selective Naked-Eye Detection of MnO_4− Directly in Aqueous Media. *ChemistrySelect* **2022**, *7* (43), No. e202203185.
(33) Jagadhane, K. S.; Bhosale, S. R.; Gunjal, D. B.; Nille, O. S.; Kolekar, G. B.; Kolekar, S. S.; Dongale, T. D.; Anbhule, P. V. Tetraphenylethene-Based Fluorescent Chemosensor with Mechanochromic and Aggregation-Induced Emission (AIE) Properties for the Selective and Sensitive Detection of Hg2+ and Ag+ Ions in Aqueous Media: Application to Environmental Analysis. *ACS Omega* **2022**, *7* (39), 34888−34900.
(34) Hong-Yun, L.; Shang-Chao, H.; Dao-Zhan, H.; Yu-Zhou, L. Synthesis, Crystal Structure and Antimicrobial Activity of (E)-2-(2-(4,8,8-Trimethyldecahydro-1,4-Methanoazulen-9-Ylidene)Ethyl)-Benzo[d]Isothiazol-3(2H)-One. *Jiegou Huaxue* **2020**, *39* (8), 1546−1552.
(35) Sheldrick, G. M. A Short History of SHELX. *Acta Crystallogr. Sect. A Found. Crystallogr.* **2008**, *64* (1), 112−122.
(36) Farrugia, L. J. WinGX and ORTEP for Windows: An Update. *J. Appl. Crystallogr.* **2012**, *45* (4), 849−854.
(37) Macrae, C. F.; Bruno, I. J.; Chisholm, J. A.; Edgington, P. R.; McCabe, P.; Pidcock, E.; Rodriguez-Monge, L.; Taylor, R.; Van De Streek, J.; Wood, P. A. Mercury CSD 2.0 - New Features for the Visualization and Investigation of Crystal Structures. *J. Appl. Crystallogr.* **2008**, *41* (2), 466−470.
(38) Spek, A. L. Structure Validation in Chemical Crystallography. *Acta Crystallogr. Sect. D Biol. Crystallogr.* **2009**, *65* (2), 148−155.
(39) Suman, G. R.; Pandey, M.; Chakravarthy, A. S. J. Review on New Horizons of Aggregation Induced Emission: From Design to Development. *Materials Chemistry Frontiers* **2021**, *5*, 1541−1584.
(40) Zhu, C.; Kwok, R. T. K.; Lam, J. W. Y.; Tang, B. Z. Aggregation-Induced Emission: A Trailblazing Journey to the Field of Biomedicine. *ACS Appl. Bio Mater.* **2018**, *1* (6), 1768−1786.
(41) He, Z.; Ke, C.; Tang, B. Z. Journey of Aggregation-Induced Emission Research. *ACS Omega.* **2018**, *3*, 3267−3277.
(42) Xia, M.; Li, C.; Liu, L.; He, Y.; Li, Y.; Jiang, G.; Wang, J. A Fast-Response AIE-Active Ratiometric Fluorescent Probe for the Detection of Carboxylesterase. *Biosensors* **2022**, *12* (7), 484.
(43) Rodrigues, A. C. B.; Pina, J.; Dong, W.; Forster, M.; Scherf, U.; Seixas De Melo, J. S. Aggregation-Induced Emission in Phenothiazine-TPE and -TPAN Polymers. *Macromolecules* **2018**, *51* (21), 8501−8512.
(44) Du, W.; Liu, X.; Liu, L.; Lam, J. W. Y.; Tang, B. Z. Photoresponsive Polymers with Aggregation-Induced Emission. *ACS Appl. Polym. Mater..* **2021**, *3*, 2290−2309.
(45) Siddharth, K.; Alam, P.; Hossain, M. D.; Xie, N.; Nambafu, G. S.; Rehman, F.; Lam, J. W. Y.; Chen, G.; Cheng, J.; Luo, Z.; Chen, G.; Tang, B. Z.; Shao, M. Hydrazine Detection during Ammonia Electro-Oxidation Using an Aggregation-Induced Emission Dye. *J. Am. Chem. Soc.* **2021**, *143* (5), 2433−2440.
(46) Wu, Z.; Fang, W.; Wu, C.; Corrigan, N. A.; Zhang, T.; Xu, S.; Boyer, C. An Aqueous Photo-Controlled Polymerization under NIR Wavelengths: Synthesis of Polymeric Nanoparticles through Thick Barriers. *Chem. Sci.* **2022**, *13*, 11519.
(47) Shen, X. Y.; Wang, Y. J.; Zhao, E.; Yuan, W. Z.; Liu, Y.; Lu, P.; Qin, A.; Ma, Y.; Sun, J. Z.; Tang, B. Z. Effects of Substitution with Donor-Acceptor Groups on the Properties of Tetraphenylethene Trimer: Aggregation-Induced Emission, Solvatochromism, and Mechanochromism. *J. Phys. Chem. C* **2013**, *117* (14), 7334−7347.
(48) Xiong, J.; Wang, K.; Yao, Z.; Zou, B.; Xu, J.; Bu, X. H. Multi-Stimuli-Responsive Fluorescence Switching from a Pyridine-Functionalized Tetraphenylethene AIEgen. *ACS Appl. Mater. Interfaces* **2018**, *10* (6), 5819−5827.
(49) Yoon, S. J.; Park, S. Polymorphic and Mechanochromic Luminescence Modulation in the Highly Emissive Dicyanodistyrylbenzene Crystal: Secondary Bonding Interaction in Molecular Stacking Assembly. *J. Mater. Chem.* **2011**, *21* (23), 8338−8346.
(50) Luo, X.; Zhao, W.; Shi, J.; Li, C.; Liu, Z.; Bo, Z.; Dong, Y. Q.; Tang, B. Z. Reversible Switching Emissions of Tetraphenylethene Derivatives among Multiple Colors with Solvent Vapor, Mechanical, and Thermal Stimuli. *J. Phys. Chem. C* **2012**, *116* (41), 21967−21972.
(51) Chi, Z.; Zhang, X.; Xu, B.; Zhou, X.; Ma, C.; Zhang, Y.; Liu, S.; Xu, J. Recent Advances in Organic Mechanofluorochromic Materials. *Chem. Soc. Rev.* **2012**, *41* (10), 3878−3896.
(52) Li, H.; Chi, Z.; Xu, B.; Zhang, X.; Li, X.; Liu, S.; Zhang, Y.; Xu, J. Aggregation-Induced Emission Enhancement Compounds Containing Triphenylamine-Anthrylenevinylene and Tetraphenylethene Moieties. *J. Mater. Chem.* **2011**, *21* (11), 3760−3767.
(53) Khoza, P. B.; Moloto, M. J.; Sikhwivhilu, L. M. The Effect of Solvents, Acetone, Water, and Ethanol, on the Morphological and Optical Properties of ZnO Nanoparticles Prepared by Microwave. *J. Nanotechnol.* **2012**, *2012*, 1.
(54) Mathivanan, M.; Tharmalingam, B.; Anitha, O.; Lin, C. H.; Thiagarajan, V.; Murugesapandian, B. All-in-One Type ESIPT-Active Multi-Stimuli Responsive 7-Diethylamino-4-Hydroxycoumarin-Rhodamine B Hydrazone as Molecular Switches and the Reversible Photochromic Features of Its Zinc Ensemble. *Mater. Chem. Front.* **2021**, *5* (23), 8183−8196.
(55) Feng, N.; Gao, C.; Guo, C. Y.; Chen, G. Copper-Phenylacetylide Nanobelt/Single-Walled Carbon Nanotube Composites: Mechanochromic Luminescence Phenomenon and Thermoelectric Performance. *ACS Appl. Mater. Interfaces* **2018**, *10* (6), 5603−5608.
(56) Ito, S.; Nagai, S.; Ubukata, T.; Ueno, T.; Uekusa, H. Relationship between Crystal Structure, Crystal Morphology, and Mechanochromic Luminescence of Triphenylimidazolylbenzothiadiazole Derivatives. *Cryst. Growth Des.* **2020**, *20* (7), 4443−4453.

https://doi.org/10.1021/acs.cgd.3c00002
Cryst. Growth Des. 2023, 23, 4164−4179

(57) Huang, B.; Gu, X.; Feng, Y.; Zhang, Y.; Jiang, D.; Chen, W. C.; Dai, G.; Ji, Y.; Zhao, Q.; Lee, C. S. Solid-State Fluorophore Based on π-Extended Heteroaromatic Acceptor: Polymorphism, Mechanochromic Luminescence, and Electroluminescence. *Cryst. Growth Des.* **2020**, *20* (4), 2454−2461.
(58) El-Gezawy, H.; Rettig, W.; Lapouyade, R. Solvatochromic Behavior of Donor - Acceptor-Polyenes: Dimethylamino-Cyano-Diphenylbutadiene. *J. Phys. Chem. A* **2006**, *110* (1), 67−75.
(59) *Validation of Analytical Procedures: Text and Methodology Q2(R1); ICH Harmonised Tripartite Guideline*; International Conference on Harmonisation of Technical Requirements for Registration of Pharmaceuticals for Human Use.
(60) Haldar, U.; Lee, H. Il. BODIPY-Derived Multi-Channel Polymeric Chemosensor with PH-Tunable Sensitivity: Selective Colorimetric and Fluorimetric Detection of Hg2+ and HSO4- in Aqueous Media. *Polym. Chem.* **2018**, *9* (39), 4882−4890.
(61) Hussain, S.; Muhammad Junaid, H.; Tahir Waseem, M.; Rauf, W.; Jabbar Shaikh, A.; Anjum Shahzad, S. Aggregation-Induced Emission of Quinoline Based Fluorescent and Colorimetric Sensors for Rapid Detection of Fe3+ and 4-Nitrophenol in Aqueous Medium. *Spectrochim. Acta - Part A Mol. Biomol. Spectrosc.* **2022**, *272*, No. 121021.
(62) Chang, M. J.; Kim, K.; Kang, C.; Lee, M. H. Enhanced Aggregability of AIE-Based Probe through H 2 S-Selective Triggered Dimerization and Its Applications to Biological Systems. *ACS Omega* **2019**, *4* (4), 7176−7181.
(63) Jung, M. J.; Kim, S. J.; Lee, M. H. ∝-Extended Tetraphenylethylene Containing a Dicyanovinyl Group as an Ideal Fluorescence Turn-On and Naked-Eye Color Change Probe for Hydrazine Detection. *ACS Omega* **2020**, *5* (43), 28369−28374.

https://doi.org/10.1021/acs.cgd.3c00002
Cryst. Growth Des. 2023, 23, 4164−4179